Int. J. Heat Mass Transfer. Vol. 33, No. 6, pp. 1135–1147, 1990
Printed in Great Britain

0017–9310/90 $3.00 + 0.00

Gravity-assisted melting in a spherical enclosure: effects of natural convection

SANJAY K. ROY and SUBRATA SENGUPTA
Department of Mechanical Engineering, University of Miami, Coral Gables, FL 33124, U.S.A.

(*Received* 3 *February* 1989 *and in final form* 8 *August* 1989)

Abstract—A theoretical model of gravity-assisted melting in a spherical enclosure is discussed in this paper. A sphere with a phase change material initially in the solid phase at its melting temperature is instantaneously exposed to a uniform higher temperature at the wall. The solid phase is assumed to have a higher density as compared to the liquid and drops down as it melts. The effects of natural convection on the melting process have been considered in this analysis. Suitable simplifications have been made where necessary, in order to reduce computational effort and time. The non-dimensional melt time and heat transfer coefficient have been obtained as a function of the property values, operating temperatures and physical size for $Md \ll 1$, $Ste \ll 1$, $10^4 \leqslant Gr \leqslant 10^6$, $10 \leqslant Pr \leqslant 100$, $0.5 \leqslant Mt \leqslant 5.0$, $0 \leqslant Sb \leqslant 0.75$, $0.01 \leqslant 1/Pr\alpha^\circ \leqslant 1.0$ and $0.01 \leqslant Ste/c_p^\circ \leqslant 0.2$. Natural convection is found to limit the range of applicability of previously published correlations.

INTRODUCTION

MANY ENGINEERING problems involve solid–liquid phase change heat transfer. Examples of phase change phenomena are manufacturing processes such as casting and welding, environmental phenomena such as freezing and thawing of soil and lakes, purification of semiconductors, manufacture of frozen food, thermal energy storage using phase change materials, melting and freezing of snow around pipes, etc. The use of latent heat thermal energy storage for solar energy applications has recently been of considerable interest because of its advantages. These include a high storage density and uniform temperature at which the energy is released. Extensive reviews on heat transfer related to this field have been published recently [1–3].

One of the most common geometries associated with thermal storage systems is the spherical capsule [4, 5]. Simplified models of gravity-assisted melting in spheres where the effects of natural convection have not been considered have been published previously [6–9]. However, the effects of natural convection are not completely understood, and in this paper, complete solutions including these additional effects are presented. Design correlations have also been developed based on these results.

DESCRIPTION OF MODEL

Figure 1 shows the geometry for the problem. Experiments [9, 10] have shown the formation of two distinct liquid regions as the solid drops down. One is a thin liquid region below the solid core from where the liquid is continuously forced out by the weight of the solid to the second larger liquid zone. For convenience, these two regions will be referred to as the '(lower) liquid film' and the '(upper) liquid zone'. Since the mode of heat transfer is quite different in the two zones, they will be analyzed separately in this paper. However, the following assumptions apply to both regions.

(1) The melting process is axisymmetric. Experimental studies on the melting process in spherical [9] and cylindrical [11] capsules with a uniform wall temperature confirm that the process is indeed symmetric.

(2) The phase change material has constant properties, except for density in the body force term, which is assumed to vary linearly with temperature. This assumption is valid when the temperature difference within the domain is not very high.

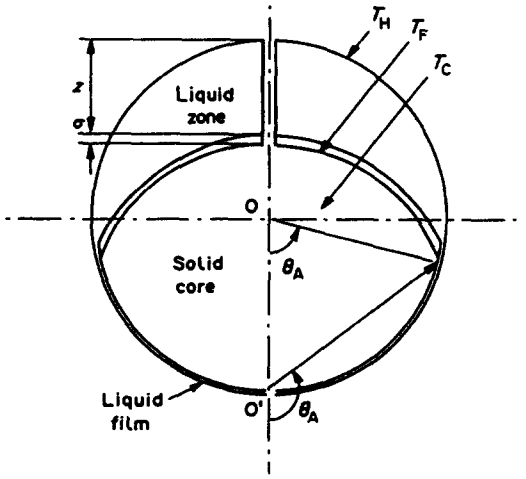

FIG. 1. The geometry.

NOMENCLATURE

Ar Archimedes number, $(\rho_s-\rho_l)gD^3/(\rho\nu^2)$
c_p specific heat at constant pressure
D diameter
F function of θ, equation (11)
Gr Grashof number, $g\beta(T_H-T_F)D^3/\nu^2$
g gravitational constant
h heat transfer coefficient
k thermal conductivity
l latent heat of fusion
Md non-dimensional parameter, equation (2)
Mt non-dimensional parameter, equation (1)
Nu Nusselt number, $qD/k(T_H-T_C)$
Pr Prandtl number, ν/α
p pressure (not including hydrostatic pressure)
q heat flux
R transformed radial coordinate
r radial coordinate
Ste Stefan number, $c_p(T_H-T_F)/l$
T temperature
t time
v velocity
z drop of solid core.

Greek symbols
α thermal diffusivity
β coefficient of thermal expansion
δ film thickness in lower region, r_o-r_i
ζ position of interface at $\theta=\pi$
Θ transformed angular coordinate
θ azimuthal angular coordinate in spherical polar coordinate
θ_A angle defining junction between upper and lower zones
σ melt thickness at $\theta=\pi$
ϕ angle made by normal with vertical axis
ψ stream function
ω vorticity.

Superscripts and subscripts
° non-dimensional property ratio (liquid/solid)
a average (area)
C cold (initial temperature of solid core)
F fusion (melting)
i inner (interface)
l liquid
m mean (area and time)
n normal direction to interface
o outer (wall)
s solid
t top (upper zone).

Note: symbols refer to liquid property values unless defined otherwise.

(3) No mushy region is formed during the melting process. The presence of a macroscopically sharp interface is expected during the melting of a pure substance.

LOWER FILM SOLUTION

Given the assumptions in the earlier section, the governing equations describing the melting process can be formulated. The following non-dimensional variables are used [11]:

$$r^*, z^*, s^* = r/D, z/D, s/D, \quad t^* = \frac{vt}{Mt\,D^2}$$

$$T^* = \frac{T-T_F}{T_H-T_F}$$

$$p^* = \frac{p}{\Delta\rho gD} \quad \text{or} \quad P^* = \frac{p-p_{hs}}{\Delta\rho gD}$$

$$v^* = \frac{Mt\,Md\,\rho^\circ Dv}{\nu}, \quad m^* = \frac{Dm}{Mt\,\rho_s\nu}$$

where m is the mass melting per unit area per unit time, P the pressure including the hydrostatic pressure p_{hs}, r_i the position of the interface, r_o the location of the outer wall, s the length measured along the interface, T_F the melting temperature of the solid phase change material, T_H the temperature of the enclosure wall during the melting process, v the velocity of liquid, and z the drop of the solid core; the superscipt ° refers to the liquid to solid property ratio, and Mt and Md are two non-dimensional parameters associated with film melting in the absence of natural convection [11]

$$Mt = \left(\left[\frac{Ste\,\rho^\circ}{Pr}\right]^3 Ar_s\right)^{-0.25} = \left(\left[\frac{k\Delta T}{l}\right]^3 \frac{\Delta\rho gD^3}{\rho_s^4\nu^5}\right)^{-0.25} \quad (1)$$

$$Md = \left(\frac{Ste\,\rho^\circ}{Pr}\Big/ Ar_s\right)^{0.25} = \left[\frac{k\Delta T\nu}{l\Delta\rho gD^3}\right]^{0.25}. \quad (2)$$

For solar energy applications, Md, Sb, $Ste\,\rho^\circ/Pr$, $Ste \ll 1$, $Mt \simeq 0.1$–10 and $Ar, Gr \gg 1$. Based on these values, the governing equations are identical to those

used previously [6], except for additional buoyancy terms in the Navier–Stokes equations when natural convection is important. Natural convection in the film will affect the melting process when the parameter Gr/Ar is of order 1 [11], i.e. when the temperature difference between the wall and the melting temperature of the phase change material is high. Also, if the density difference between the solid and the liquid phases is very small, Gr/Ar may be quite large and once again natural convection will affect the heat transfer. The Navier–Stokes equations in the film including these buoyancy terms are given below [11].

Film momentum equations (Navier–Stokes equations)

$$\frac{Gr}{Ar} T\cos\theta = \frac{\partial p}{\partial r} \tag{3}$$

$$Md\frac{1}{r^2}\frac{\partial}{\partial r}\left[r^2\frac{\partial v_\theta}{\partial r}\right]+\frac{Gr}{Ar}T\sin\theta = \frac{1}{r}\frac{\partial p}{\partial\theta} \tag{4}$$

with the boundary conditions

$$r_o = 0.5, \quad r = r_o : \vec{v} = 0, \quad r = r_i : v_\theta = 0$$

where δ is the film thickness $r_o - r_i$.

Method of solution

The method of solution is an extension of the solution technique originally developed for the cylindrical geometry by Bareiss and Beer [10], and later used for the spherical geometry by Roy and Sengupta [6] and Bahrami and Wang [8]. When natural convection effects ($Gr/Ar = 0$) are negligible, the solution for the melt rate is given by [6]

$$\frac{dz}{dt} = \left[-\frac{c'}{4}\frac{1}{(c-1)}\right]^{0.25} \tag{5}$$

where c is a constant of integration given by

$$\left[c-\left[\frac{5+3\cos^2\theta_A}{8}\right]\right] = (c-\cos\theta_A)^{3/4}(c-1)^{1/4} \tag{6}$$

and c' is

$$c' = \frac{1}{r}\frac{\partial}{\partial r}\left[r^2\frac{\partial v_\theta}{\partial\theta}\right] = -\tfrac{1}{3}(1-\cos\theta_A)(2+\cos\theta_A). \tag{7}$$

This equation is further simplified by using the geometric condition

$$z = \cos\theta_A \tag{8}$$

and the final solution is

$$\frac{dz}{dt} = \left[\frac{1}{12}\frac{(1-z)(2+z)}{(c-1)}\right]^{0.25}. \tag{9}$$

A solution method identical to the one used when $Gr/Ar = 0$ can be used if it is possible to show that

$$\frac{\partial p}{\partial\theta} - \frac{Gr}{Ar}Tr\sin\theta = \text{Function of } \theta \text{ only}. \tag{10}$$

On integrating the momentum equation in the radial direction

$$p = -\frac{Gr}{Ar}\cos\theta\int T\,dr + F(\theta) \tag{11}$$

the pressure gradient in the angular direction is therefore

$$\frac{\partial p}{\partial\theta} = \frac{Gr}{Ar}\left[\sin\theta\int T\,dr - \cos\theta\frac{\partial}{\partial\theta}\int T\,dr\right]+\frac{dF}{d\theta}$$

$$= \frac{Gr}{Ar}\left[\frac{\ln r - 1}{r_i - r_o}r_i r_o\sin\theta\right.$$

$$\left.+\frac{dr_i}{d\theta}\frac{\ln r - r/r_o}{(r_i-r_o)^2}r_o^2\cos\theta\right]+\frac{dF}{d\theta}. \tag{12}$$

For $Md \ll 1$, r is approximately equal to 0.5 since δ is very small, and so the pressure gradient becomes

$$\frac{\partial p}{\partial\theta} = \frac{dF}{d\theta} = \frac{Gr}{Ar}\left[\frac{1-\ln 0.5}{4}\right]\frac{d}{d\theta}\left[\frac{\cos\theta}{\delta}\right]. \tag{13}$$

The constant c' is therefore

$$c' = \left[\frac{dF}{d\theta} - \frac{Gr}{Ar}\left[\frac{1-\ln 0.5}{4}\right]\frac{d}{d\theta}\left[\frac{\cos\theta}{\delta}\right]\right]\sin\theta. \tag{14}$$

Integrating for the function F, we obtain

$$F(\theta) = F(\theta_A) + c'(\ln(\tan\theta/2) - \ln(\tan\theta_A/2))$$

$$+\frac{Gr}{Ar}\left[\frac{1-\ln 0.5}{4}\right]\left[\frac{\cos\theta}{\delta} - \frac{\cos\theta_A}{\delta(\theta_A)}\right]. \tag{15}$$

The boundary condition for pressure ($p = 0$ at $\theta = \theta_A$ [6]) may be applied at the enclosure wall or the interface to find the value for $F(\theta_A)$

$$p(\theta_A) = 0 \tag{16}$$

or

$$F(\theta_A) = \frac{Gr}{Ar}\left[\frac{1-\ln 0.5}{\delta(\theta_A)}\cos\theta_A + \frac{\cos\theta_A}{2}\right]. \tag{17}$$

Thus, the pressure distribution is given by

$$p = c'\ln(\tan(\theta/2)) - \ln(\tan(\theta_A/2))$$

$$+\frac{Gr}{Ar}\left[\frac{\cos\theta_A}{2}\right]. \tag{18}$$

Now, using the same procedure as in the solution for $Gr/Ar = 0$, the constant c' becomes

$$c' = -\tfrac{1}{2}(1-\cos\theta_A)(2+\cos\theta_A)$$

$$+\frac{1}{2}\frac{Gr}{Ar}\cos\theta_A(1+\cos\theta_A). \tag{19}$$

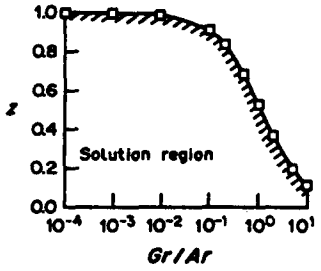

FIG. 2. Range of film solution for different values of Gr/Ar.

The final solution is therefore

$$\frac{dz}{dt} = \left(\frac{1}{c-1}\left[\frac{(1-z)(2+z)}{12} - \frac{Gr}{Ar}\frac{z(1+z)}{8}\right]\right)^{0.25}. \quad (20)$$

Discussion

The solution for the drop rate brings out an extremely important point. The film solution is found to be applicable only as long as

$$z \leqslant -0.5+\sqrt{(0.25+2/(1+1.5Gr/Ar))}. \quad (21)$$

This limiting value of z and the region of validity of the film solution is given in Fig. 2. Beyond this point the solution fails, as the rate of drop of the solid core becomes zero. The film thickness gradually increases after this, since once $dz/dt \to 0$, $d\delta/dt \to m/\rho_s$ and the film thickness continuously increases. Thus the film solution can no longer be used to predict the position of the interface beyond this point.

The effect of natural convection is to increase the pressure and thus the total force acting in the upward direction (equation (18)). As a result, the film thickness increases, and the heat transfer and the melt rate are reduced. Figure 3 shows the effect of Grashof number on the melt rate. The melt remains almost identical to the zero Gr case for the most part but tends to slow down at the final stages of melting. Such a trend had also been noticed previously by Bareiss and Beer [10] in their experimental study of melting in a cylindrical enclosure. However, they were unable to give any explanation for this difference in melt rate.

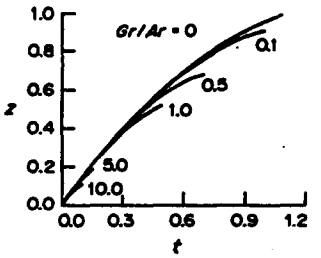

FIG. 3. Film solution for drop vs time for different Gr/Ar: the ends of lines indicate the limits of validity of the film solution.

SOLUTION IN UPPER LIQUID ZONE

In the liquid zone, it is necessary to use the same reference quantities for length, time, temperature and melt flux since these are based on the overall melting process. However, the reference quantities for velocity and pressure need to be changed since the characteristic dimension of the liquid region is different from that in the film. Since the flow is buoyancy driven in the liquid zone, for moderate to high Grashof numbers, the velocity can be non-dimensionalized as follows:

$$\bar{v}^* = \bar{v}/(\sqrt{(Gr)}v/D). \quad (22)$$

There is no obvious reference pressure in this case, and it is convenient to use the reference pressure used for the film.

A complete analysis of the melting process including the heat transfer at the upper surface of the solid core requires the study of both the upper and lower liquid zones. Since the process is quite different in the two regions, and a relatively simple closed-form solution is available for the lower region, it is advantageous to modify this solution where necessary and couple it with results of a numerical model of the upper region. Thus, the governing equations can be written as

$$\frac{1}{Mt}\frac{\partial T}{\partial t} + \sqrt{(Gr)}\bar{v}\cdot\nabla T = \frac{1}{Pr}\nabla^2 T \quad (23)$$

$$\frac{1}{Mt}\frac{\partial \omega}{\partial t} + \sqrt{(Gr)}\bar{v}\cdot\nabla\omega = \nabla^2\omega + \sqrt{(Gr)}T(\nabla\times\bar{g}) \quad (24)$$

$$-\omega = \nabla^2\psi \quad (25)$$

$$v_r = \frac{1}{r^2\sin\theta}\frac{\partial\psi}{\partial\theta}, \quad v_\theta = \frac{-1}{r\sin\theta}\frac{\partial\psi}{\partial r} \quad (26)$$

$$\frac{dz}{dt} = \left(\frac{1}{c-1}\left[\frac{(1-\zeta)(2+\zeta)}{12} - \frac{Gr}{Ar}\frac{\zeta(1+\zeta)}{8}\right]\right)^{0.25} \quad (27)$$

$$\zeta = 1 - r_i(\theta = \pi) = z + \sigma \quad (28)$$

where ψ is the Stokes stream function, ω the vorticity, ζ the interface location and σ the melt thickness at $\theta = \pi$. When there is no melting at the upper surface, $\sigma = 0$, and $\zeta = z$. A few points must be noted at this point.

(a) Since the problem is axisymmetric, and the governing equations in the upper liquid region cannot be simplified, the stream function–vorticity formulation of the governing equations has been used above.

(b) Equation (27), the solution from the earlier section, describing the rate of drop of the solid core, has been modified to account for the melting at its upper surface.

(c) Melting occurs at the upper surface of the solid core, but experiments show that the surface remains approximately spherical [9]. This has also been veri-

fied numerically as discussed later. Thus, the melt thickness at the upper surface is assumed to be constant and equal to σ (equation (28)).

(d) A coordinate system with the origin at the center of the sphere used to obtain the film solution will create complications when used with a numerical model because of the possibility of having more than one boundary point along a coordinate line [9]. A coordinate system with the origin at the bottom of the sphere, used by Prasad and Sengupta [12], is therefore used for the analysis of the upper liquid zone.

(e) In the film solution, the pressure at the upper surface of the solid core has been assumed to be equal to the hydrostatic pressure. Thus, a correction term may be required for the pressure forces acting on the solid core. The values for pressure at the interface for $\theta > \theta_A$ can be obtained by solving the primitive equations in the upper zone. These equations can be written as

$$\bar{\nabla} p = \frac{Gr^{0.5}}{Ar}\left[-\frac{1}{Mt}\frac{\partial \bar{v}}{\partial t} - Gr^{0.5}\,\bar{v}\cdot\bar{\nabla}\bar{v} + \bar{\nabla}^2\bar{v} + Gr^{0.5}\,Tg\right]. \tag{29}$$

Careful consideration of the above equations shows that the effects of pressure at the upper surface on the drop rate will be relatively small for most cases. At the interface, the velocity of the liquid is of order $1/Mt\sqrt{(Gr)}$. Thus, the convective terms are small and can be neglected. Since the temperature of the fluid at the interface is equal to the melting point, the buoyancy forces are also equal to zero. The pressure gradient along the interface is therefore balanced by the shear stresses and is therefore very small compared to the pressure gradient in the film. Consequently, the effects of pressure at the upper surface are neglected in this analysis.

No generalized solutions are available for the Navier–Stokes equation. The governing equations for the upper region therefore need to be solved numerically. The boundary conditions for the upper region are dependent on the melting taking place at the lower surface and thus have to be carefully analyzed. This is discussed in greater detail in the following section.

Method of solution

Two important features of the upper liquid zone, the irregular shape and the change in this shape with time, complicate the numerical model. The domain is fixed by an algebraic transformation to simplify the solution technique

$$R = \frac{r - r_i}{r_o - r_i}, \quad \Theta = \frac{\theta - \theta_A}{\pi - \theta_A}, \quad t = t.$$

As a result, the governing equations now become

$$\frac{1}{Mt}\frac{\partial T}{\partial t} = \frac{A}{Pr}\frac{\partial^2 T}{\partial R^2} + \frac{2B}{Pr}\frac{\partial^2 T}{\partial R\,\partial\Theta} + \frac{C}{Pr}\frac{\partial^2 T}{\partial\Theta^2} + \left[D1 + \frac{D2}{Pr}\right]\frac{\partial T}{\partial R} + \left[E1 + \frac{E2}{Pr}\right]\frac{\partial T}{\partial\Theta} \tag{30}$$

$$\frac{1}{Mt}\frac{\partial\omega}{\partial t} = A\frac{\partial^2\omega}{\partial R^2} + 2B\frac{\partial^2\omega}{\partial R\,\partial\Theta} + C\frac{\partial^2\omega}{\partial\Theta^2} + (D1+D2)\frac{\partial\omega}{\partial R} + (E1+E2)\frac{\partial\omega}{\partial\Theta} + F\omega + G1\frac{\partial T}{\partial R} + G2\frac{\partial T}{\partial\Theta} \tag{31}$$

$$\frac{1}{C_\beta}\omega = A\frac{\partial^2\psi}{\partial R^2} + 2B\frac{\partial^2\psi}{\partial R\,\partial\Theta} + C\frac{\partial^2\omega}{\partial\Theta^2} + D\frac{\partial\psi}{\partial R} - E2\frac{\partial\psi}{\partial\Theta} \tag{32}$$

$$v_r = C_\alpha\left[X\frac{\partial\psi}{\partial R} + Y\frac{\partial\psi}{\partial\Theta}\right], \quad v_\theta = C_\beta\left[Z\frac{\partial\psi}{\partial R}\right] \tag{33}$$

where A, B, etc. are transformation coefficients.

Boundary conditions

The boundary conditions for the upper zone depend on the melting taking place at the film. To be able to put the velocity at the junction between the lower and the upper zones equal to zero, the characteristic velocity of the liquid in the film must be much smaller than the characteristic velocity in the liquid zone. For typical solar thermal systems, this ratio is

$$0.1 < \frac{v_f}{v_t} = \frac{1}{Mt\,Md\,\rho^\circ\sqrt{(Gr)}} < 10 \tag{34}$$

where v_f is the liquid velocity in the film and v_t the liquid velocity in the upper zone. Thus, the boundary velocities cannot be neglected in the liquid zone and the streamlines will intersect the interface as it drops down. Keeping this point in mind, the boundary conditions are derived.

Enclosure wall and axis of symmetry. The boundary conditions for the no-slip wall and the symmetry axis are similar to those used in a variety of fluid dynamics problems. The value of the stream function is zero throughout, as is the vorticity along the symmetry axis. At the enclosure wall, the vorticity boundary condition is obtained by using a Taylor series expansion for the second-order gradient [13]

$$\frac{\partial^2\psi}{\partial R^2} = \frac{2}{(\Delta R)^2}\psi_{w-1} \tag{35}$$

and by using a finite difference form for the cross derivative

$$\frac{\partial^2\psi}{\partial R\,\partial\Theta} = \frac{-1}{2\Delta R\Delta\Theta}(\psi_{w-1,\theta+1}\,\psi_{w-1,\theta-1}). \tag{36}$$

All other terms are zero in the vorticity definition equation which can now be evaluated. The temperature gradient along the symmetry axis is zero.

Solid–liquid interface. At the interface, the total velocity is due to two factors: the downward movement of the core and the density difference between the solid and liquid phases. Since the volume of the enclosure is assumed to be a constant, the second

component must be neglected. The normal velocity at the interface is therefore given by

$$v_n = \frac{1}{Mt}\frac{1}{\sqrt{(Gr)}}\frac{dz}{dt}\cos\phi \tag{37}$$

where ϕ is the angle between the normal at the interface and the vertical axis. The radial and angular velocities are therefore

$$v_r = v_n\cos(\phi-\theta), \quad v_\theta = v_n\sin(\phi-\theta). \tag{38}$$

From the stream function definition equations it is possible to show that

$$\frac{\partial\psi}{\partial\Theta} = \frac{1}{XY}\left[\frac{Z}{C_\beta}v_r - \frac{Y}{C_\alpha}v_\theta\right]. \tag{39}$$

This equation is numerically integrated using the boundary condition that the stream function is zero at $\Theta = 1$.

Since both components of velocity are non-zero in this case, the complete vorticity equation has to be used to obtain the boundary values. One-sided differencing is used to solve the vorticity equation.

Film–liquid zone junction. The fluid velocities at the junction are not known since the coordinate system differs in the film solution. However, the form of the angular velocity can be assumed to be identical

$$v_\theta = K(r+b+c/r) \tag{40}$$

and the stream function is therefore given by

$$\psi = -K\sin\theta_A\left[\tfrac{1}{3}(r^3-r_o^3)+\frac{b}{2}(r^2-r_o^2)+c(r-r_o)\right]. \tag{41}$$

The velocity and the stream function are known to be zero at the outer wall, and the velocity and the stream function values are known at the interface. Thus, the values of the coefficients are

$$b = -(r_i-r_o)+K_1 \tag{42}$$

$$c = -r_o(-r_o+K_1) \tag{43}$$

$$\frac{1}{K_1} = 3\left[\frac{2}{r_i v_{\theta i}\sin\theta_A(r_i-r_o)}\psi_i+1\right] \tag{44}$$

$$K = \frac{v_{\theta i}}{K_1}\Big/\left[1-\frac{r_o}{r_i}\right]. \tag{45}$$

The vorticity is once again found by using the complete vorticity definition equation and the temperature is assumed to vary linearly from the interface to the wall.

Initial conditions. If all terms in the momentum and energy transport equations ((30) and (31)) are multiplied by Mt, it immediately becomes obvious that the terms accounting for the rate of change of vorticity and temperature in a control volume ($\partial\omega/\partial t$ and $\partial T/\partial t$) are of order 1 and are certainly much smaller than a typical convective term for moderate to high Gr. Thus, these terms may be neglected and a 'quasi-steady' solution for different values of ζ may be obtained in the upper region. It is possible to use a 'quasi-steady' solution since the interface remains almost spherical even after melting takes place at the upper surface [9]. Besides reducing the CPU time required, there are some additional advantages of using such a scheme.

(a) Different numbers of grid points can be used very easily for different values of ζ. Thus, finer grids can be used when ζ is large in order to obtain realistic solutions.

(b) In the unsteady solutions, it was necessary to start the solution after ζ reached a certain arbitrary value, which could be as high as 0.2, to avoid stability problems. It is difficult to estimate the total melt volume at the upper surface for small ζ. Using the 'quasi-steady' solution, it is possible (and in fact, necessary) to extrapolate for times when a solution is unavailable. It is also possible to obtain solutions for considerably smaller values of ζ with relatively less effort.

(c) Since the upper liquid zone becomes uncoupled from the interface equations (but not vice versa), Md is no longer a parameter while solving the 'quasi-steady' model. Thus, fewer computer runs will be required.

In order to obtain the quasi-steady solution, the flow field is assumed to be completely stagnant at the start of the numerical solution. The boundary condition for velocity at the interface and the junction between the upper zone and the liquid film is obtained from the drop rate so that the flow profile in the domain is realistic. Thus, even though the boundary is fixed, liquid comes into the domain from the film and goes out at the interface, and the streamlines will intersect the interface.

Solution algorithm

The governing equations are converted into finite difference forms using central differences for the space derivatives and forward differences for the time derivatives. At the boundaries, one-sided first order differences are used where central second order space derivatives are not available. These sets of difference equations are then solved using an explicit algorithm.

(a) New values of temperature are obtained by solving the energy equations in the liquid using the values available from the earlier time step.

(b) New values for vorticity are similarly obtained by solving the vorticity transport equation using old values for all variables except temperature.

(c) Using these values of vorticity, the vorticity definition equation is solved using an SOR scheme to obtain new values for the stream function.

(d) The velocities and the boundary vorticities are calculated using these stream function values.

(e) Steps (a)–(d) are repeated until quasi-steady state is achieved.

A hopscotch algorithm for parabolic and elliptic equa-

tions with cross-derivatives [14] was also used in some preliminary runs in an attempt to reduce computational time. Though it was possible to use larger time steps using this method, errors were slightly greater, and the explicit scheme discussed above was therefore used throughout the study.

Verification

Extensive verification of the model and computer code has been done. The computer code was written to solve the complete model in an unsteady fashion as was done earlier by Prasad and Sengupta [12]. In order to reduce computer time requirements, a few modifications were made later to obtain the 'quasi-steady' model. Verification of this code was achieved as follows.

(a) Results for conduction and natural convection in a concentric spherical annulus were obtained. The natural convection results have been compared with the analytical solution of Mack and Hardee [15], and the maximum difference in Nusselt number is less than 10%.

(b) The film solution was also obtained by running the unsteady model with Gr, Pr, and Gr/Ar equal to zero and using a melt time step of 10^{-4}. The difference in the results was negligible.

(c) 'Quasi-steady' solutions have been compared with a completely unsteady solution for $\zeta = 0.3$ and 0.56 with the parameters $Ar_s = 5 \times 10^6$, $Ste\,\rho^\circ/Pr = 2 \times 10^{-3}$, $Gr = 5 \times 10^5$, $Pr = 50$ and $Gr/Ar = 0.1$. The difference can be seen to be small in Fig. 4.

(d) In order to verify that the effects of pressure at the upper surface are negligible, an unsteady solution was obtained using the parameters in (c), except with $Gr/Ar = 0.0$. The change in melt time was negligible.

(e) Grid size and time-step independence of the unsteady solution have been checked by considering cases with a 26×26 grid with a time step of 2.5×10^{-8}, a 21×21 grid with a time step of 5×10^{-8} and a 21×21 grid with a time step of 2.5×10^{-8}. The difference in melt time was negligible.

(f) Both (sensible) heat balance and mass balance in the upper liquid zone alone have been checked during the unsteady solution and it was found that:

$$\frac{\text{Heat in} - \text{Heat out} - \text{Heat stored in liquid}}{\text{Heat in}} \simeq 5\% \tag{46}$$

$$\frac{\text{Melt at lower surface} - \text{Mass added to upper surface}}{\text{Melt at lower surface}} < 1\%. \tag{47}$$

If the overall heat balance which includes the energy used to melt the solid phase at the lower surface is included, the net heat unaccounted for is much smaller than 5% and is negligible for all cases. Complete details are given in Roy [16].

Discussion

The parameters in this problem are Ar_s, $Ste\,\rho^\circ/Pr$, Gr, Pr, and Gr/Ar. The first two, Ar_s and $Ste\,\rho^\circ/Pr$, are always used as the melt time and melt distance parameters, Mt and Md. Since Md does not affect the liquid region in the 'quasi-steady' model, this parameter can be dropped. Also, since the effect of pressure at the upper surface is small, Gr/Ar was not

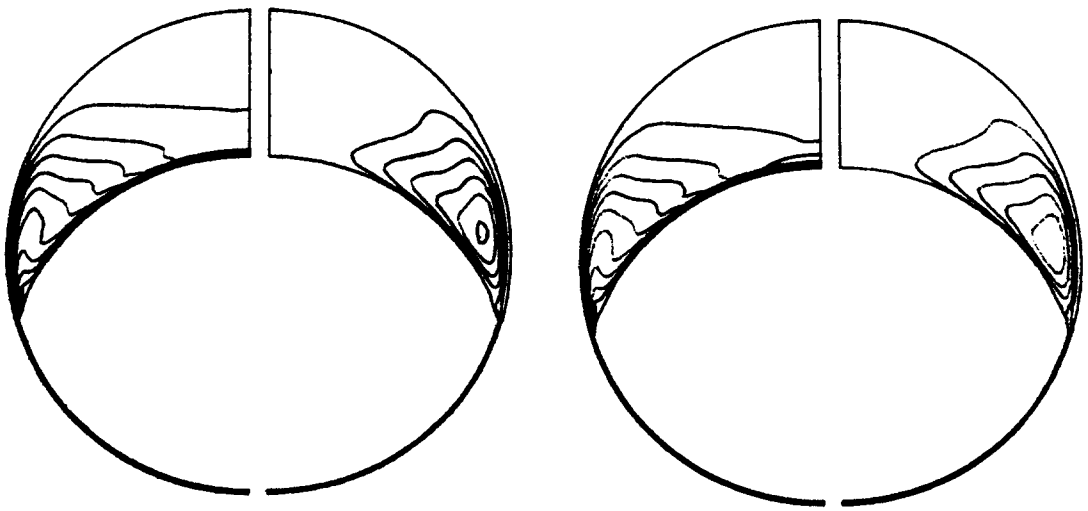

FIG. 4. Comparison of unsteady and quasi-steady solutions: stream function and temperature distribution. $Ar_s = 5 \times 10^6$, $Ste\,\rho^\circ/Pr = 2 \times 10^{-3}$, $Gr = 5 \times 10^5$, $Pr = 50$, $Gr/Ar = 0.1$.

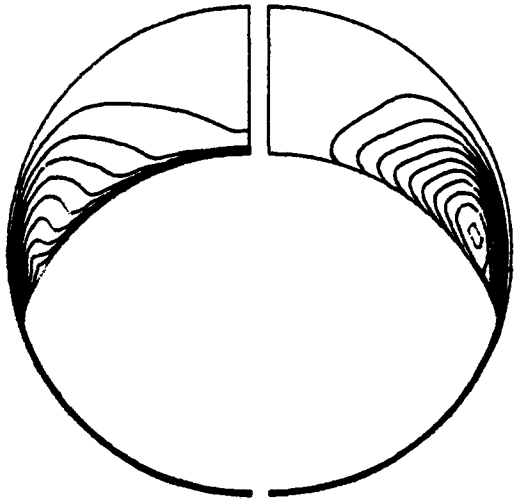

Fig. 5. Stream function and temperature distribution. $Gr = 10^5$, $Pr = 50$, $Mt = 1.0$, $\zeta = 0.3$.

considered in this study. Nusselt numbers used in this study have been defined as follows:

$$Nu = qD/k(T_H - T_C) \quad (48)$$

where q is the heat flux (with subscript i for interface, a for average at the wall at any time t, and m for mean, averaged over the entire melting period, at the wall). Results have been obtained for ranges of parameters usually encountered in solar thermal energy systems. Mt has been varied from 0.5 to 5.0, Gr from 10^4 to 10^6 and Pr from 10 to 100 for ζ ranging from 0.1 to 0.9; 21×21 grids have been used for all cases where $\zeta \leqslant 0.3$ and 31×21 grids have been used in other cases. Time steps varying from 5.0×10^{-7} to 5×10^{-8} have been used as required in order to obtain stable realistic solutions.

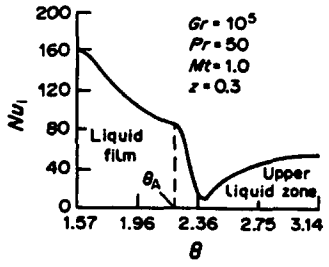

Fig. 6. Interface Nusselt number distribution.

Before the effects of the different parameters are discussed separately, some general observations about the flow in the liquid region can be made.

(a) A large stagnant region of hot fluid develops above the solid core near $\theta = \pi$ (Fig. 5). This has been noted previously by others (e.g. refs. [17, 18]) in experiments with cylindrical geometry. Unfortunately, such results are not available for the spherical geometry. Because of this hot fluid, the interface Nusselt number in this region is quite high (Fig. 6).

(b) The downward velocity of the solid core has a very large impact on the flow field in many cases. This point has not been reported to date.

(c) The local wall Nusselt number in the upper region was in general much lower ($< 10\%$) than the wall Nusselt number in the film region.

Grashof number effects. From Fig. 7, the flow pattern can be seen to be strongly affected by Gr. As Gr increases, the effect of the solid core moving downward reduces and the hot fluid from the film tends to flow upwards and closer to the wall near $\theta = \theta_A$. When Gr reduces, the velocity due to the downward motion of the solid core becomes increasingly important. As

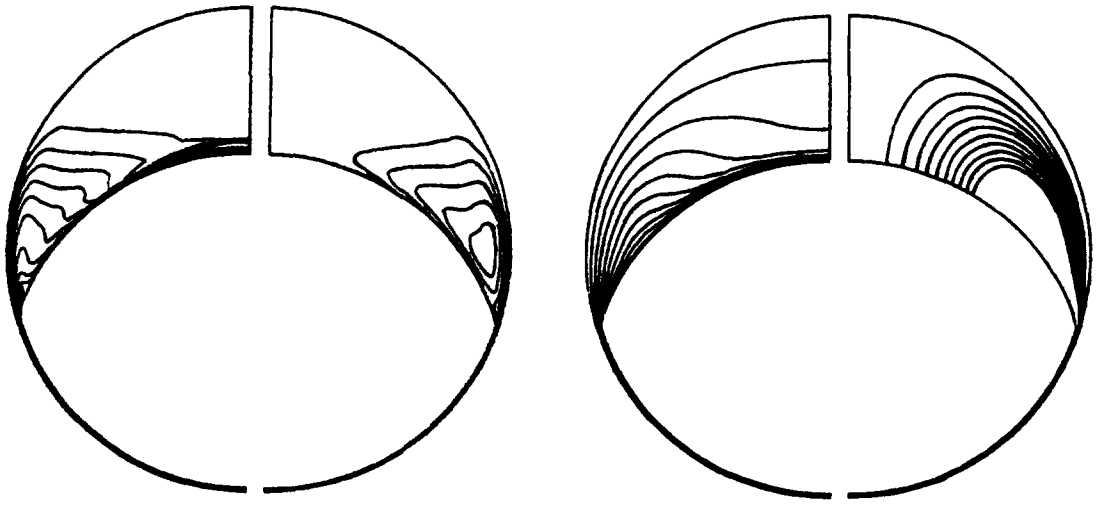

Fig. 7. Effects of Grashof number: stream function and temperature distribution. $Pr = 50$, $Mt = 1.0$, $\zeta = 0.3$.

a consequence, the temperature gradient at the outer wall near $\theta = \pi$ decreases. However, since the wall Nu is low in this region, it does not affect the overall heat transfer coefficient significantly. Thus, the parameter $Mt\sqrt{(Gr)}$, which is the ratio of the typical natural convection velocity to the solid core velocity, is not of much importance in determining the heat transfer coefficient at the outer wall even though it does have a significant qualitative effect on the flow patterns.

Prandtl number effects. The effects of Prandtl number on the fluid flow and the temperature distribution in the liquid zone can be seen in Fig. 8. For $Pr = 100$, the flow tends to be dominated to a greater extent by the solid core velocity. The higher the Prandtl number, the greater is the viscosity and the lower the effects of natural convection in the upper region. As a result, the temperature gradient and Nusselt number at the wall increase with an increase in Pr, but the change is quite small for the range of Pr which has been considered in this study.

Melt time parameter effects. Figure 9 shows the effects of the melt time parameter Mt. In order to study the effects of Mt in the upper zone, it is advantageous to consider the value of $1/Mt$ which is of the order of the downward velocity of the solid. Thus, as Mt increases, the downward velocity decreases, and

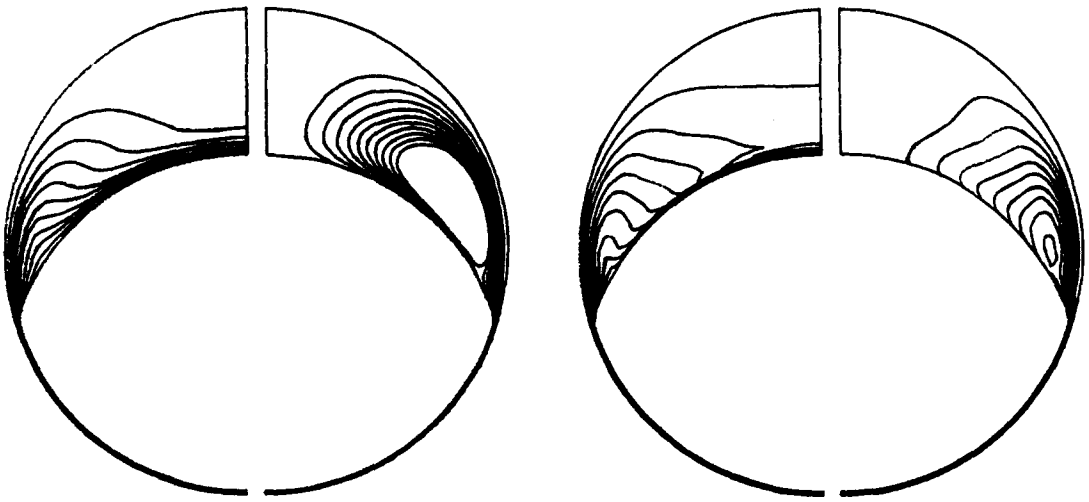

FIG. 8. Effects of Prandtl number: stream function and temperature distribution. $Gr = 10^5$, $Mt = 1.0$, $\zeta = 0.3$.

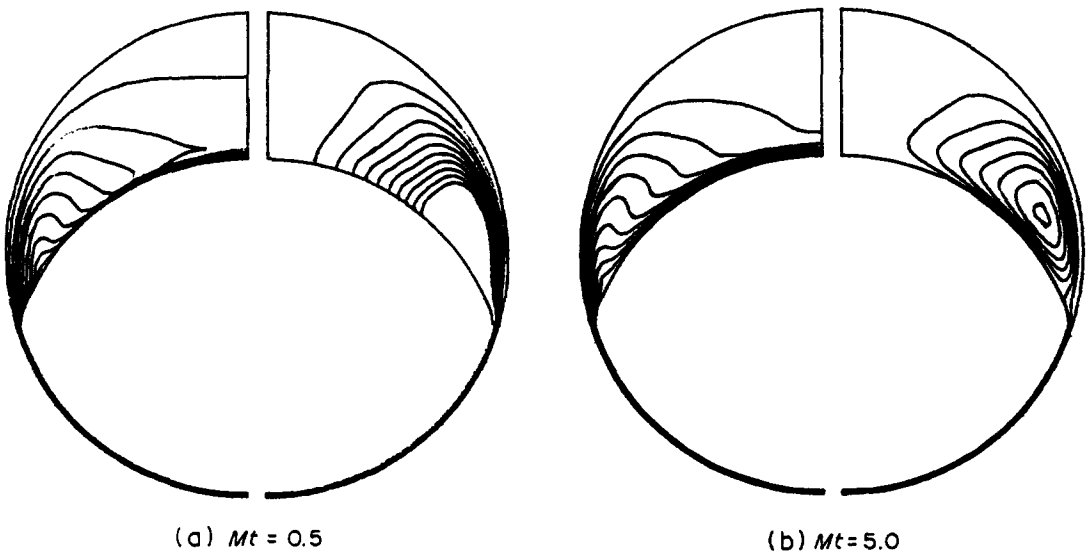

FIG. 9. Effects of melt time parameter Mt: stream function and temperature distribution. $Gr = 10^5$, $Pr = 50$, $\zeta = 0.3$.

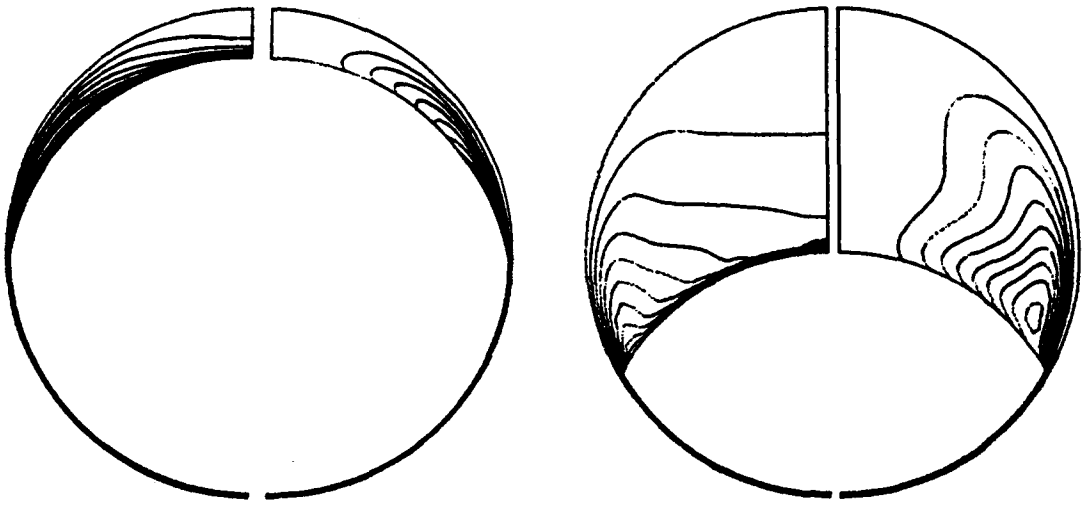

Fig. 10. Effects of interface location ζ: stream function and temperature distribution. $Gr = 10^5$, $Pr = 50$, $Mt = 1.0$.

buoyancy plays an increasing role in the liquid region. As a result, the temperature gradient near $\theta = \pi$ increases with decreasing Mt where the solid velocity is high. However, since the temperature gradient at the wall near $\theta = \theta_A$ is not really affected by the change in Mt, the overall heat transfer coefficient remains almost constant.

Drop height effects. The flow pattern in the liquid region is dependent on the size (and shape) of the liquid zone as expected (Fig. 10). When ζ is low (0.1), the distance between the wall and the solid core is small and so the temperature gradient and Nusselt number at the wall are quite high. As melting progresses, the Nusselt number rapidly drops as the temperature gradient continuously decreases at the wall.

DEVELOPMENT OF CORRELATIONS

In order that the results of this study may be easily used in the actual design of storage systems, it is necessary to obtain correlations for the important design parameters. Of particular interest are the variation of the overall Nusselt number and the rate at which the solid interface drops down during the melting process.

Drop rate and time

The location of the interface at $\theta = \pi$ is given by

$$\frac{d\zeta}{dt} = \frac{dz}{dt} + \frac{d\sigma}{dt} \tag{49}$$

where $d\sigma/dt$ is the melt rate at the interface at $\theta = \pi$

$$\frac{d\sigma}{dt} = Md\, Nu_i(\theta = \pi). \tag{50}$$

It would be convenient to obtain $d\sigma/dt$, and thus $Nu_i(\theta = \pi)$ as a direct function of dz/dt, so that this term can simply be dropped from the final correlation if natural convection effects need to be ignored. Keeping this in mind, a multiple linear regression analysis was done using the Nusselt numbers obtained from the numerical study ($10^4 \leqslant Gr \leqslant 10^6$, $10 \leqslant Pr \leqslant 100$, $0.5 \leqslant Mt \leqslant 5.0$). The following equation with a maximum error of about 5% was obtained for the Nusselt number at $\theta = \pi$:

$$Nu_i(\theta = \pi) = 2.945 Gr^{0.13}\, Pr^{0.31}\, Mt^{-0.13} \frac{dz}{dt}. \tag{51}$$

It is interesting to note that the Nusselt number is independent of the position of the interface ζ, except for the effect of dz/dt itself. Also, if we note that $Pr/Mt \simeq Ste/Md$ when $\rho^\circ \to 1$ (which is the approximation used in the upper liquid region to maintain mass balance), the Nusselt number is

$$Nu_i(\theta = \pi) = 2.945 Gr^{0.13}\, Pr^{0.18} (Ste/Md)^{0.13} \frac{dz}{dt}. \tag{52}$$

Thus, the effect of heat transfer to the liquid in the film (which is directly proportional to Ste/Md) on the melt rate at the upper surface is of the same order as the effect due to heat transfer at the upper wall (a function of Gr and Pr). The effect of Rayleigh number ($= Gr\, Pr$) itself is quite small ($Nu \propto Ra^{0.13}\, Pr^{0.05}$) when compared to other spherical geometries where $Nu \propto Ra^{0.25}$ [19]. This is probably due to the fact that the outer wall is heated in this case, whereas the inner body is usually at a higher temperature for other typical spherical geometries. For $Sb < 0.75$ and $Md \ll 1$, equation (51) can be modified to include the effects of

subcooling

$$\frac{d\zeta}{dt} = \frac{dz}{dt}[1+2.945Gr^{0.13}\,Pr^{0.31}\,Mt^{-0.13}\,Md(1-Sb)] \tag{53}$$

dz/dt is approximately independent of subcooling [7] and is given by equation (27)

$$\frac{dz}{dt} = \left(\frac{1}{c-1}\left[\frac{(1-\zeta)(2+\zeta)}{12} - \frac{Gr}{Ar}\frac{(1+\zeta)}{8}\right]\right)^{0.25} \tag{54}$$

where c is given by the real root of the cubic equation

$$\left[c-\left[\frac{5+3\zeta}{8}\right]\right] = (c-\zeta)^{3/4}(c-1)^{1/4}. \tag{55}$$

Equations (53)–(55) can now be used to estimate the drop rate for the following range of parameter values:

$$10^4 \leqslant Gr \leqslant 10^6, \quad 10 \leqslant Pr \leqslant 100, \quad 0.5 \leqslant Mt \leqslant 5.0$$

$$Md \ll 1, \quad Ste \ll 1, \quad 0.05 \leqslant z \leqslant 0.9$$

$$Sb < 0.75, \quad Gr/Ar \ll 1.$$

In order to obtain the drop height as a function of time, it is necessary to integrate the above equation. This is somewhat complicated and a simplified correlation can be derived from equations (54) and (55)

$$\frac{dz}{dt} = 1.636 - 1.700\zeta + 1.425\zeta^2 - 0.093\zeta^3. \tag{56}$$

The time and interface positions can be obtained from

$$t = (0.686\zeta + 0.023\zeta^2 + 0.355\zeta^3)/(1+C) \tag{57}$$

$$\zeta = (1.546t - 0.770t^2 + 0.135t^3)(1+C) \tag{58}$$

where

$$C = 2.945Gr^{0.13}\,Pr^{0.31}\,Mt^{0.13}\,Md(1-Sb). \tag{59}$$

Results obtained by the correlation given above have been compared with the experimental data of Moore [20] in Fig. 11. The error is greater than that obtained using the simplified film solution alone due to the additional melting at the upper surface. Bahrami and Wang [8] have suggested that the difference between their results and the experimental data is due to an error in the reported Stefan number. A closer examination of the experimental data [20] also tends to confirm this argument [16] since the thickness of the glass enclosure used in their experiments was of the same order as the film thickness.

Average wall Nusselt number

The average wall Nusselt number at any time t (equation (48)) can be derived by considering the Nusselt numbers at the lower and upper surfaces separately. At the lower surface, the average Nusselt number for $\theta \leqslant \theta_A$ is

$$Nu_a = \frac{dz}{dt}\frac{(1+\zeta)}{2}\frac{(1+0.5Ste)}{Md}. \tag{60}$$

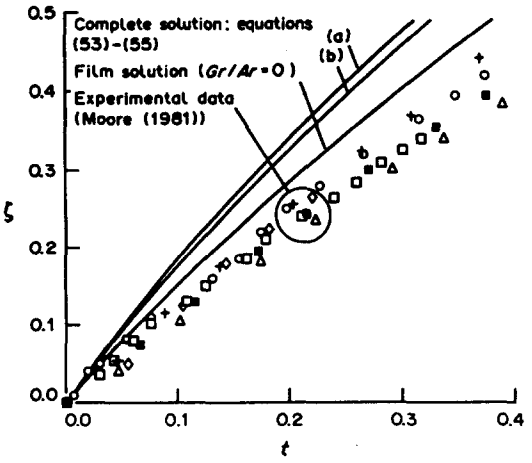

FIG. 11. Comparison of numerical results with experimental data. □○△ (a): $Md = 3.6\times10^{-3}$, $Mt = 4.3$, $Gr = 5.4\times10^5$, $Gr/Ar = 0.11$. +◇⊠ (b): $Md = 4.3\times10^{-3}$, $Mt = 2.6$, $Gr = 1.2\times10^6$, $Gr/Ar = 0.24$.

The average Nusselt number at the wall in the upper region is a function of Mt, Gr, Pr, z and dz/dt. Once again, it is advantageous to obtain Nu_a as a direct function of dz/dt. A third order curve was used to account for the variation with z, and a multiple regression analysis then gave the following relation with a maximum error of about 10%:

$$Nu_a = 1.308Gr^{0.22}\,Pr^{0.08}\,Mt^{0.15}(1-3.47\zeta + 4.69\zeta^2 - 1.68\zeta^3)\frac{dz}{dt}. \tag{61}$$

The average Nusselt number over the complete surface after taking the effects of subcooling into account therefore becomes

$$Nu_a = \frac{1}{2}\frac{dz}{dt}\left[\frac{(1-Sb+0.5Ste)}{Md}(1-\zeta^2) + 1.308Gr^{0.22}\,Pr^{0.08}\,Mt^{0.15}(1-Sb)\cdot(1-2.47\zeta+1.22\zeta^2+3.01\zeta^3)\right]. \tag{62}$$

The mean wall Nusselt number (equation (48)) averaged over the entire melt time can be evaluated by integrating until $t = t(\text{melt})$ or $\zeta = 1$ and dividing by the time (or $\zeta = 1$) to give

$$Nu_m = \left[\frac{(1-Sb+0.5Ste)/6Md + 1.21Gr^{0.22}\,Pr^{0.08}\,Mt^{0.15}(1-Sb)}{1+2.945Gr^{0.13}\,Pr^{0.31}\,Mt^{-0.13}\,Md(1-Sb)}\right]\times(1+Ste_s) \tag{63}$$

where Ste_s is the solid Stefan number $(c_{ps}(T_F-T_C)/l)$. The additional term is required to account for the excess heat required to raise the temperature of the core to the melting temperature.

As discussed before, when $Sb \neq 0$ most of the heat transfer to the core takes place when $t < 0.05$. Thus, the correlations for Nu_a as a function of ζ are valid only after approximately 5% of the melt when $0 < Sb \leqslant 0.75$. Higher values of subcooling are not expected since this would imply a very high Ste_s, which would defeat the purpose of using a latent heat thermal storage system. The other ranges of parameters for the correlations are

$$10^4 \leqslant Gr \leqslant 10^6, \quad 10 \leqslant Pr \leqslant 100, \quad 0.5 \leqslant Mt \leqslant 5.0$$
$$Md \ll 1, \quad Ste \ll 1, \quad Gr/Ar \leqslant 0.1$$
$$0.05 \leqslant z \leqslant 0.9, \quad Sb < 0.75.$$

The estimated overall errors for the above correlations are of the order of 5%. However, experimental confirmation is required.

It should also be noted that all the above correlations have been developed so that individual effects of subcooling, natural convection in the film and natural convection in the upper region can be easily separated out from the primary conduction heat transfer in the film. Each of these are described by separate terms which can be dropped if necessary.

CONCLUSIONS

The effects of natural convection on the melting process of an unfixed phase change material in a spherical enclosure with an isothermal boundary has been investigated. Numerical results and correlations have been obtained for the specific case when Md and $Ste \ll 1$ for the range of parameters encountered in typical solar thermal applications. A few general conclusions can be drawn from this study.

(a) Natural convection affects the flow and pressure distribution in the film. The parameter Gr/Ar, which is the ratio of the buoyancy force due to density variation of the liquid with temperature and the density difference between the two phases, reduces the melt rate and places an upper bound for the range over which the film solution is valid.

(b) The fluid flow and heat transfer process in the upper liquid region are essentially quasi-steady, since the liquid velocity in both the film and the upper zone are much greater than the rate of movement of the interface.

(c) In the upper zone, the flow field is strongly affected by the downward motion of the solid core, particularly for low Gr and high Pr.

(d) The heat transfer at the upper wall is much smaller than the heat transfer through the liquid film for all cases.

(e) A significant amount (15% for typical cases) of melting takes place at the upper surface of the solid core. This is a function of the Grashof and Prandtl numbers as well as the sensible heat input to the liquid in the film.

(f) The effects of Grashof number and Prandtl number in the upper region are small ($Nu \propto Ra^{0.13} Pr^{0.05}$) when compared to natural convection effects in commonly encountered spherical geometries where $Nu \propto Ra^{0.25}$ [19].

REFERENCES

1. R. Viskanta, Phase-change heat transfer. In *Solar Heat Storage: Latent Heat Materials* (Edited by G. Lane), Vol. I, pp. 153–222. CRC Press, Boca Raton, Florida (1983).
2. R. Viskanta, Natural convection in melting and solidification. In *Natural Convection: Fundamentals and Applications* (Edited by S. Kakac *et al.*), pp. 845–877. Hemisphere, Washington, DC (1985).
3. S. Sengupta and S. K. Roy, Gravity-assisted melting in enclosures. In *Energy Storage Systems* (Edited by B. Kilkis and S. Kakac), NATO ASI Publ. Ser. E, pp. 721–752. Kluwer, Dordrecht (1989).
4. Anon., Molten balls could store latent heat, *The Engineer (Lond.)* **263**(6804–05), 100–101 (1986).
5. T. Saitoh and K. Hirose, High-performance phase-change thermal energy storage using spherical capsules, ASME Paper 84-HT-8 (1984).
6. S. K. Roy and S. Sengupta, The melting process in spherical enclosures, *J. Heat Transfer* **109**, 460–462 (1987).
7. S. K. Roy and S. Sengupta, Melting of a free solid in a spherical enclosure: effect of subcooling, *J. Solar Energy Engng* **110**, 32–36 (1989).
8. P. A. Bahrami and T. G. Wang, Analysis of gravity and conduction-driven melting in a sphere, *J. Heat Transfer* **109**, 806–809 (1987).
9. F. Moore and Y. Bayazitoglu, Melting within a spherical enclosure, *J. Heat Transfer* **104**, 19–23 (1982).
10. M. Bareiss and H. Beer, An analytical solution of the heat transfer process during melting of an unfixed solid phase change material inside a horizontal enclosure, *Int. J. Heat Mass Transfer* **27**, 739–746 (1984).
11. S. K. Roy and S. Sengupta, A generalized model for gravity-assisted melting in enclosures. *J. Heat Transfer* (1990), in press.
12. A. Prasad and S. Sengupta, Numerical investigation of melting inside a horizontal cylinder including the effects of natural convection, *J. Heat Transfer* **109**, 803–806 (1987).
13. P. J. Roache, *Computational Fluid Dynamics*, pp. 140–146. Hermosa, New Mexico (1976).
14. A. R. Gourlay and S. McKee, The construction of hopscotch methods for parabolic and elliptic equations in two space dimensions with a mixed derivative, *J. Comp. Appl. Math.* **3**, 201–206 (1977).
15. L. R. Mack and M. C. Hardee, Natural convection between concentric spheres at low Rayleigh numbers, *Int. J. Heat Mass Transfer* **11**, 387–396 (1968).
16. S. K. Roy, Melting in spherical enclosures, Ph.D. Dissertation, Department of Mechanical Engng, University of Miami, Florida (1988).
17. M. K. Moallemi and R. Viskanta, Melting around a migrating heat source, *J. Heat Transfer* **107**, 451–458 (1985).
18. M. K. Moallemi and R. Viskanta, Experiments on fluid flow induced by melting around a migrating heat source, *J. Fluid Mech.* **157**, 35–51 (1985).
19. G. D. Raithby and K. G. T. Hollands, A general method of obtaining approximate solutions of laminar and turbulent free convection problems. In *Advances in Heat Transfer* (Edited by T. F. Irvine and J. P. Hartnett), Vol. 11, pp. 266–315. Academic Press, New York (1975).
20. F. Moore, Melting within a spherical enclosure, M.S. Thesis, Rice University, Texas (1981).

FUSION ASSISTEE PAR LA PESANTEUR DANS UNE CAVITE SPHERIQUE—EFFETS DE LA CONVECTION NATURELLE

Résumé—Un modèle théorique est discuté pour la fusion assistée par la pesanteur, dans une cavité sphérique. Une sphère contenant une phase solide, initialement à la température de fusion, est instantanément exposée sur la paroi à une température uniforme plus élevée. La phase solide est supposée avoir une densité plus élevée que le liquide et les gouttes tombent pendant la fusion. L'effet de la convection naturelle sur le mécanisme de fusion est considéré dans cette analyse. Des simplifications convenables sont faites, si nécessaire, de façon à réduire le temps et les difficultés de calcul. Le temps adimensionnel de fusion et le coefficient de transfert thermique sont obtenus en fonction des paramètres thermophysiques, des températures opératoires pour $Md \ll 1$; $Ste \ll 1$; $10^4 \leqslant Gr \leqslant 10^6$; $10 \leqslant Pr \leqslant 100$; $0{,}5 \leqslant Mt \leqslant 5{,}0$; $0 \leqslant Sb \leqslant 0{,}75$; $0{,}01 \leqslant 1/Pr\,\alpha^\circ \leqslant 1{,}0$ et $0{,}01 \leqslant Ste/c_p^\circ \leqslant 0{,}2$. On trouve que la convection naturelle limite le domaine d'application des formules précédemment publiées.

EINFLUSS DER NATÜRLICHEN KONVEKTION AUF DAS SCHWERKRAFTUNTERSTÜTZTE SCHMELZEN IN EINEM KUGELFÖRMIGEN HOHLRAUM

Zusammenfassung—In dieser Arbeit wird ein theoretisches Modell für das schwerkraftunterstützte Schmelzen in einem kugelförmigen Hohlraum diskutiert. Eine Kugel aus Phasenwechselmaterial befindet sich anfänglich in festem Zustand bei Schmelztemperatur und wird plötzlich einer gleichförmigen höheren Temperatur an der Wand ausgesetzt. Es wird angenommen, daß die feste Phase eine größere Dichte als die flüssige hat und daher beim Schmelzen herabsinkt. Die Einflüsse der natürlichen Konvektion auf den Schmelzvorgang werden in der vorliegenden Analyse berücksichtigt. Geeignete Vereinfachungen werden vorgenommen, falls dies notwendig erscheint, um Berechnungsaufwand und -zeit zu verringern. Es ergibt sich die dimensionslose Schmelzzeit und der Wärmeübergangskoeffizient in Abhängigkeit von Stoffeigenschaften, Arbeitstemperaturen und physikalischen Größen: $Md \ll 1$, $Ste \ll 1$, $10^4 \leqslant Gr \leqslant 10^6$, $10 \leqslant Pr \leqslant 100$, $0{,}5 \leqslant Mt \leqslant 5{,}0$, $0 \leqslant Sb \leqslant 0{,}75$, $0{,}01 \leqslant 1/Pr\,\alpha^\circ \leqslant 1{,}0$ und $0{,}01 \leqslant Ste/c_p^\circ \leqslant 0{,}2$. Es zeigt sich, daß die natürliche Konvektion den Anwendungsbereich früher veröffentlichter Korrelationen begrenzt.

ПЛАВЛЕНИЕ В СФЕРИЧЕСКОЙ ПОЛОСТИ ПРИ ВОЗДЕЙСТВИИ СИЛЫ ТЯЖЕСТИ: ЭФФЕКТ ЕСТЕСТВЕННОЙ КОНВЕКЦИИ

Аннотация—Обсуждается теоретическая модель плавления в сферической полости в поле силы тяжести. Материал, первоначально находящийся в твердой фазе при температуре плавления, мгновенно подвергается действию более высокой постоянной температуры у стенки. Предполагается, что твердая фаза имеет большую плотность по сравнению с жидкостью и отрывающимися по мере плавления каплями. Анализируется влияние естественной конвекции на процесс плавления. С целью сокращения затрачиваемого на расчеты времени сделаны соответствующие упрощения. Определены безразмерное время плавления и коэффициент теплопереноса в зависимости от значений характерных величин, рабочих температур и физического размера при $Md \ll 1$; $Ste \ll 1$; $10^4 \leqslant Gr \leqslant 10^6$; $10 \leqslant Pr \leqslant 100$; $0{,}5 \leqslant Mt \leqslant 5{,}0$; $0 \leqslant Sb \leqslant 0{,}75$; $0{,}01 \leqslant 1/Pr\,\alpha^\circ \leqslant 1{,}0$ $0{,}01 \leqslant Ste/c_p^\circ \leqslant 0{,}2$. Найдено, что естественная конвекция ограничивает область применения ранее опубликованных соотношений.